Aerobic Oxidation of Primary Alcohols (Including Methanol) by Copper(II)− and Zinc(II)−Phenoxyl Radical Catalysts

Phalguni Chaudhuri,* Martina Hess, Jochen Müller, Knut Hildenbrand, Eckhard Bill, Thomas Weyhermüller, and Karl Wieghardt*

Contribution from the Max-Planck-Institut für Strahlenchemie, Stiftstrasse 34-36, D-45470 Mülheim a.d. Ruhr, Germany

Received May 5, 1999

Abstract: The tetradentate ligand *N*,*N*′-bis(3,5-di-*tert*-butyl-2-hydroxyphenyl)-1,2-phenylenediamine, H_4L^1, has been prepared, and its square planar complexes $[Cu^{II}(L^3)]$ and $[Zn^{II}(L^3)]$ have been synthesized from the reaction of H_4L^1 with $[Cu^I(NCCH_3)_4](ClO_4)$ or $Zn(BF_4)_2{\cdot}2H_2O$ in methanol in the presence of air. The dianion $(L^3)^{2-}$ represents the two-electron oxidized form of $(L^1)^{4-}$, namely *N*,*N*′-bis(3,5-di-*tert*-butyl-2-hydroxyphenyl)-1,2-diiminoquinone. Complexes $[Cu^{II}(L^3)]{\cdot}CH_3CN$ and $[Zn(L^3)]{\cdot}CH_3CN$ have been characterized by X-ray crystallography, EPR spectroscopy, and magnetochemistry; $[Cu^{II}(L^3)]$ has an $S = {}^1/_2$ ground state, and $[Zn(L^3)]$ is diamagnetic. Cyclic voltammetry established that both complexes undergo two successive reversible one-electron oxidations and two successive reversible one-electron reductions. Thus, the coordinated ligand exists in five oxidation levels. The species $[M^{II}(L^4)]PF_6$ (M = Cu^{II}, Zn^{II}) and $[M^{II}(L^5)](ClO_4)_2$ (M = Cu^{II}, Zn^{II}) have been isolated and characterized by UV/vis, EPR, and ^1H NMR spectroscopy and by magnetic susceptibility measurements, where $(L^4)^-$ represents the monoanion *N*-(3,5-di-*tert*-butyl-2-hydroxyphenyl)-*N*′-(3,5-di-*tert*-butyl-2-phenoxyl)-1,2-diiminoquinone and (L^5) is the neutral ligand *N*,*N*′-bis(3,5-di-*tert*-butyl-2-phenoxyl)-1,2-diiminoquinone. Similarly, two complexes of the type $[M^{II}(L^1H_2)]$ (M = Cu^{II}, Zn^{II}) have been isolated from the reaction of L^1H_4 with $Cu^{II}(ClO_4)_2{\cdot}6H_2O$ or $Zn(ClO_4)_2{\cdot}6H_2O$ under anaerobic conditions in the presence of NEt_3. Complexes $[Cu^{II}(L^4)]PF_6$ and $[Zn(L^4)]PF_6$ selectively oxidize primary alcohols (including methanol and ethanol) in a stoichiometric fashion under anaerobic conditions, yielding the corresponding aldehydes and $[M^{II}(L^2H_2)]^+$ (M = Cu^{II}, Zn^{II}), where $(L^2)^{3-}$ is the trianionic form of *N*,*N*′-bis(3,5-di-*tert*-butyl-2-hydroxyphenyl)-1,2-diiminosemiquinone. Since the latter reduced forms react rapidly with dioxygen with formation of $[M^{II}(L^4)]^+$ (M = Cu, Zn) and 1 equiv of H_2O_2, these oxidized species are catalysts for the air oxidation of primary alcohols, including ethanol and methanol, with concomitant formation of H_2O_2 and aldehydes. The kinetics of the stoichiometric reactions and of the catalyses (initial rate method) have been measured. Large kinetic isotope effects show that H-abstraction from the α-carbon atom of a coordinated alcoholato ligand is the rate-determining step in all cases.

Introduction

The copper-containing metalloprotein galactose oxidase (GO) is an enzyme which catalyzes selectively the aerobic oxidation of primary alcohols to aldehydes with formation of 1 equiv of hydrogen peroxide (eq 1). In the active site of the active form

$$RCH_2OH + O_2 \xrightarrow{[GO]} RCHO + H_2O_2 \qquad (1)$$

of this enzyme, a single copper(II) ion is coordinatively bound to a (thioether-modified) tyrosyl radical,[1] two histidine residues, and a tyrosinate anion (or tyrosine).[2]

The mechanism of the catalytic conversion of primary alcohols by GO is well understood.[3] In the rate-determining step, an O-coordinated alcoholate ligand undergoes an H-abstraction reaction from the α-carbon atom of the alcoholate to the coordinated tyrosyl radical, generating a bound ketyl radical anion and a tyrosine. The ketyl−radical ligand is then intramolecularly converted via a one-electron oxidation to the aldehyde with concomitant formation of a Cu^I species. Reoxidation of the latter species by O_2 regenerates the active Cu^{II}−tyrosyl form and H_2O_2 (Scheme 1).

(1) (a) Whittaker, J. W. In *Metal Ions in Biological Systems*; Sigel, H., Sigel, A., Eds.; Marcel Dekker: New York, 1994; Vol. 30, pp 315−360. (b) Knowles, P. F.; Ito, N. In *Perspectives in Bio-inorganic Chemistry*; Jai Press Ltd.: London, 1994; Vol. 2, pp 207−244.

(2) (a) Ito, N.; Phillips, S. E. V.; Stevens, C.; Ogel, Z. B.; McPherson, M. J.; Keen, J. N.; Yadav, K. D. S.; Knowles, P. F. *Nature* **1991**, *350*, 87. (b) Ito, N.; Phillips, S. E. V.; Stevens, C.; Ogel, Z. B.; McPherson, M. J.; Keen, J. N.; Yadav, K. D. S.; Knowles, P. F. *Faraday Discuss.* **1992**, *93*, 75. (c) Ito, N.; Phillips, S. E. V.; Yadav, K. D. S.; Knowles, P. F. *J. Mol. Biol.* **1994**, *238*, 794.

(3) (a) Wachter, R. M.; Montagne-Smith, M. P.; Branchaud, B. P. *J. Am. Chem. Soc.* **1997**, *119*, 7743. (b) Branchaud, B. P.; Montagne-Smith, M. P.; Kosman, D. J.; McLaren, F. R. *J. Am. Chem. Soc.* **1993**, *115*, 798. (c) Whittaker, M. M.; Whittaker, J. M. *Biophys. J.* **1993**, *64*, 762. (d) Whittaker, M. M.; Ballou, D. P.; Whittaker, J. W. *Biochemistry* **1998**, *37*, 8426. (e) Wachter, R. M.; Branchaud, B. P. *J. Am. Chem. Soc.* **1996**, *118*, 2782. (f) Whittaker, J. W.; Whittaker, M. M. *Pure Appl. Chem.* **1998**, *70*, 903.

(4) (a) Halfen, J. A.; Jazdzewski, B. A.; Mahapatra, S.; Berreau, L. M.; Wilkinson, E. C.; Que, L., Jr.; Tolman, W. B. *J. Am. Chem. Soc.* **1997**, *119*, 8217. (b) Sokolowski, A.; Leutbecher, H.; Weyhermüller, T.; Schnepf, R.; Bothe, E.; Bill, E.; Hildebrandt, P.; Wieghardt, K. *J. Biol. Inorg. Chem.* **1997**, *2*, 444. (c) Zurita, D.; Gautier-Luneau, I.; Menage, S.; Pierre, J.-L.; Saint-Aman, E. *J. Biol. Inorg. Chem.* **1997**, *2*, 46. (d) Itoh, S.; Takayama, S.; Arakawa, R.; Furuta, A.; Komatsu, M.; Ishida, A.; Takamuku, S.; Fukuzumi, S. *Inorg. Chem.* **1997**, *36*, 1407. (e) Zurita, D.; Menage, S.; Pierre, J.-L.; Saint-Aman, E. *New J. Chem.* **1997**, *21*, 1001. (f) Müller, J.; Weyhermüller, T.; Bill, E.; Hildebrandt, O.; Ould-Moussa, L.; Glaser, T.; Wieghardt, K. *Angew. Chem., Int. Ed.* **1998**, *37*, 616. (g) Halcrow, M. A.; Chia, L. M. L.; Liu, X.; McInnes, J. L.; Yellowlees, L. J.; Mabbs, F. E.; Davies, J. E. *Chem. Commun.* **1998**, 2465.

10.1021/ja991481t CCC: $18.00
Published on Web 10/04/1999

Scheme 1. Proposed Reaction Mechanism of GO, Ref 3

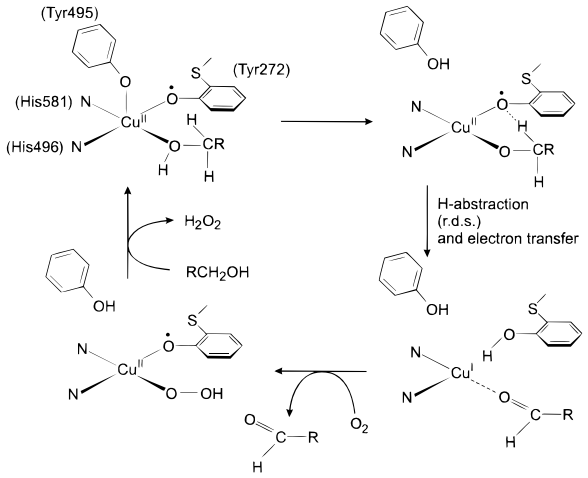

Chart 1. Catalysts for the Aerobic Oxidation of Alcohols

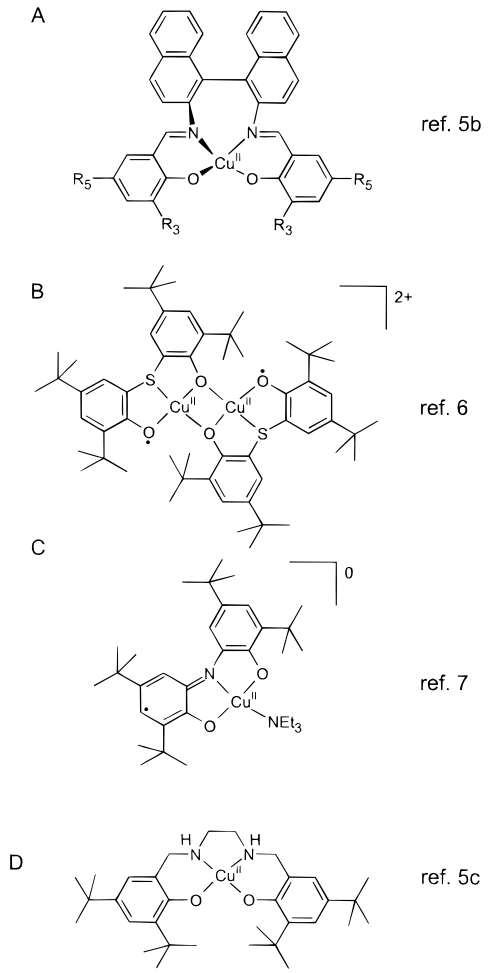

While the active form of GO containing the Cu^{II}−phenoxyl moiety has been successfully assembled in a number of low-molecular-weight structural model complexes,[4] only very few functional models have been reported[5−7] to date. Stack's[5a,b] functional models A (Chart 1) catalyze the aerobic oxidation of activated primary alcohols according to eq 1 but not that of ethanol or methanol. We have reported a model system[6] where a dinuclear Cu^{II}−phenoxyl complex B catalyzes the oxidation of primary alcohols (including ethanol but not methanol). In addition, B catalyzes also the aerobic oxidation of secondary alcohols, yielding ketones (eq 2) or pinacols (eq 3).

$$R_2CHOH + O_2 \xrightarrow{[B]} R_2C{=}O + H_2O_2 \quad (2)$$

$$2R_2CHOH + O_2 \xrightarrow{[B]} R_2C(OH){-}C(OH)R_2 + H_2O_2 \quad (3)$$

Finally, the mononuclear complex C[7] oxidizes only primary alcohols, including ethanol, by dioxygen to aldehydes and H_2O_2, and D has been reported to catalyze the electrochemical oxidation of alcohols.[5c]

Here we report two new catalysts which effectively oxidize primary alcohols, including methanol, with dioxygen to aldehydes and H_2O_2 but not secondary alcohols, such as 2-propanol or diphenylcarbinol. Cu complexes capable of catalyzing the oxidation of alcohols to aldehydes with air have been described previously, but water and not H_2O_2 is the reduction product.[8]

We have synthesized the new tetradentate ligand *N*,*N*′-bis-(3,5-di-*tert*-butyl-2-hydroxyphenyl)-1,2-phenylenediamine, H_4-(L^1), and investigated its coordination chemistry with Cu and Zn ions. This ligand exists in five oxidation levels, as shown in Scheme 2; Chart 2 lists the complexes prepared, with their labels and spin ground states.

Results

Syntheses and Characterization of Complexes. The ligand *N*,*N*′-bis(3,5-di-*tert*-butyl-2-hydroxyphenyl)-1,2-phenylenediamine, $H_4(L^1)$, has been prepared by a condensation reaction of 3,5-di-*tert*-butylcatechol and *o*-phenylenediamine (2:1) in the presence of triethylamine in *n*-heptane. Scheme 2 shows one resonance structure for each of the five oxidation states of this ligand (L^1−L^5), which are interrelated by one-electron-transfer steps. The central *o*-phenylenediamine moiety in $H_4(L^1)$ can be oxidized, yielding the iminosemiquinone, $H_3(L^2)$, and then the diiminoquinone, $H_2(L^3)$. Finally, each of the two phenols can be successively oxidized by one electron, yielding $H(L^4)$ and L^5. Note that $H_3(L^2)$ and $H(L^4)$ are radicals with an $S = {}^1/_2$ ground state, whereas the species $H_4(L^1)$, $H_2(L^3)$, and L^5 are diamagnetic. As we will show below, these five oxidation levels of the tetradentate ligands $(L^1)^{4-}$, $(L^2)^{3-}$, $(L^3)^{2-}$, $(L^4)^{-}$, and $(L^5)^0$ are accessible in their copper(II) and zinc(II) complexes (Chart 2).

The reaction of $H_4(L^1)$ with $[Cu^I(NCCH_3)_4](ClO_4)$ or Zn^{II}-$(BF_4)_2{\cdot}2H_2O$ in dry methanol in the presence of air yields microcrystalline precipitates of green $[Cu^{II}(L^3)]$ and gray-black $[Zn^{II}(L^3)]$, respectively. Recrystallization of these materials from acetonitrile afforded single crystals of $[M^{II}(L^3)]{\cdot}CH_3CN$ (M^{II} = Cu, Zn) suitable for X-ray crystallography. The structure of the neutral complex in crystals of $[Cu(L^3)]{\cdot}CH_3CN$ is shown in Figure 1; that of the zinc complex is very similar and not shown. Table 1 gives selected bond distances and angles for both complexes.

The respective divalent metal ion in $[M(L^3)]$ (M = Cu, Zn) is coordinated to the tetradentate ligand $(L^3)^{2-}$; the resulting N_2O_2M coordination polyhedron is nearly square planar. The

(5) (a) Wang, Y.; Stack, T. D. P. *J. Am. Chem. Soc.* **1996**, *118*, 13097. (b) Wang, Y.; DuBois, J. L.; Hedman, B.; Hodgson, K. O.; Stack, T. D. P. *Science* **1998**, *279*, 537. (c) Saint-Aman, E.; Menage, S.; Pierre, J.-L.; Degrancq, E.; Gellou, G. *New J. Chem.* **1998**, 393.

(6) Chaudhuri, P.; Hess, M.; Flörke, U.; Wieghardt, K. *Angew. Chem., Int. Ed.* **1998**, *37*, 2217.

(7) Chaudhuri, P.; Hess, M.; Weyhermüller, T.; Wieghardt, K. *Angew. Chem., Int. Ed.* **1999**, *38*, 1095.

(8) (a) Kitajima, N.; Whang, K.; Moro-oka, Y.; Uchida, A.; Sasada, Y. *J. Chem. Soc., Chem. Commun.* **1986**, 1504. (b) Marko, I. E.; Giles, P. R.; Tsukazaki, M.; Brown, S. M.; Urch, C. J. *Science* **1996**, *274*, 2044. (c) Marko, I. E.; Tsukazaki, M.; Giles, P. R.; Brown, S. M.; Urch, C. J. *Angew. Chem., Int. Ed. Engl.* **1997**, *36*, 2208.

Scheme 2. Oxidation Levels, Spin States, and Labels of the Ligand (Only One Resonance Structure Is Given in Each Case)

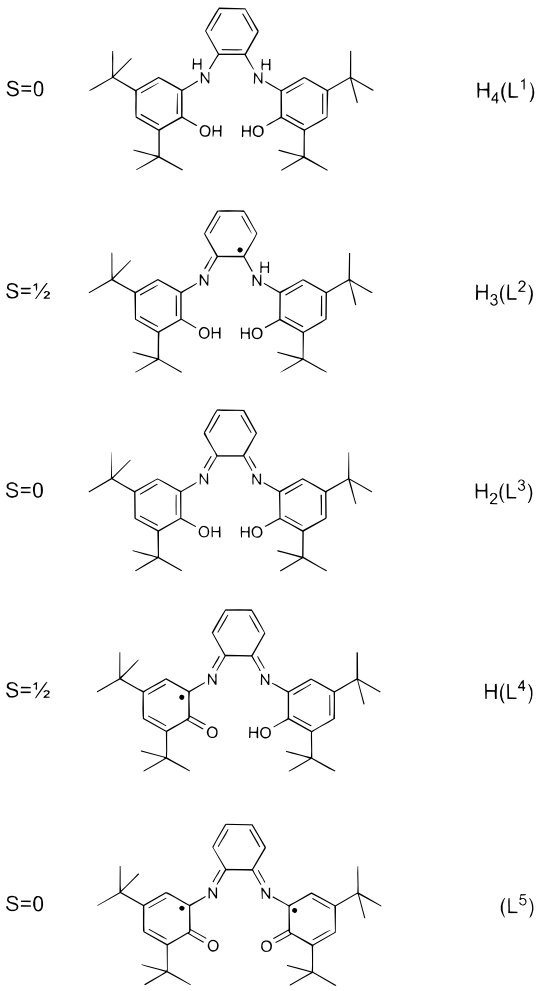

Chart 2. Complexes Prepared, with Their Labels and Their Electronic Ground States

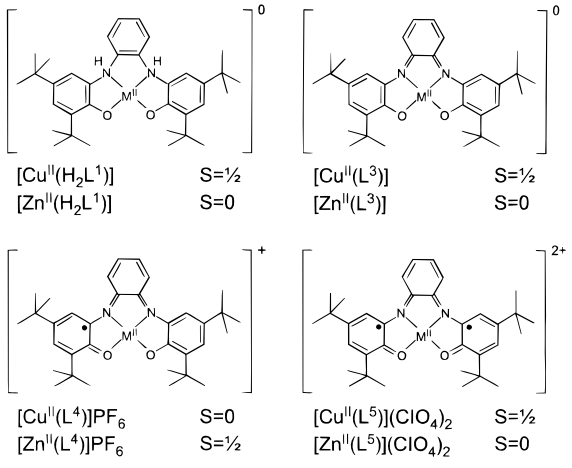

square planar Zn(II) complex in a neutral N_2O_2 coordination is unprecedented in the Cambridge Structural Database. The structure determinations unambiguously show that, in both structures, the oxidation level of the ligand is $(L^3)^{2-}$, containing a central diiminoquinone moiety and two phenolates. Thus, the distances C9−C10 and C11−C12, at 1.36 ± 0.01 Å, are significantly shorter than the distances C8−C9, C10−C11, and C12−C13, at 1.43 ± 0.01 Å, and C8−C13, at 1.47 ± 0.01 Å.

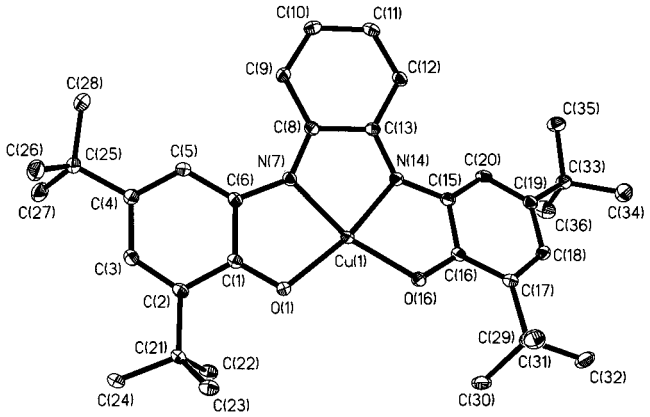

Figure 1. Structure of the neutral molecule in crystals of $[Cu^{II}(L^3)]\cdot CH_3CN$. The structure of $[Zn(L^3)]\cdot CH_3CN$ is similar and is not shown.

Table 1. Selected Bond Distances (Å) and Angles (deg)

	$[Cu(L^3)]\cdot CH_3CN$	$[Zn(L^3)]\cdot CH_3CN$
M−O1	1.918(2)	1.922(2)
M−O16	1.942(2)	1.943(2)
M−N7	1.954(2)	1.955(2)
M−N14	1.922(2)	1.923(2)
N7−C8	1.342(3)	1.345(3)
N7−C6	1.373(3)	1.370(3)
N14−C13	1.335(3)	1.328(3)
N14−C15	1.368(3)	1.377(3)
C8−C9	1.433(3)	1.436(3)
C9−C10	1.358(3)	1.365(3)
C10−C11	1.425(3)	1.431(3)
C11−C12	1.362(3)	1.362(3)
C12−C13	1.425(3)	1.432(3)
O1−C1	1.307(3)	1.311(3)
O16−C16	1.318(3)	1.320(3)
N7−M−N14	83.17(7)	83.05(8)
N14−M−O16	84.12(7)	84.31(7)
O16−M−O1	109.59(6)	109.42(6)
O1−M−N7	84.65(7)	84.74(7)
C6−N7−C8	134.8(2)	135.0(2)
C6−N7−M	112.1(1)	112.1(2)
C8−N7−M	113.0(1)	112.8(1)
C13−N14−C15	134.1(2)	133.9(2)
C13−N14−M	114.1(1)	114.6(1)
C15−N14−M	111.8(1)	111.4(1)

Correspondingly, the imino C═N bonds, at 1.34 ± 0.01 Å, are shorter than the C−N bonds to the phenolates, at 1.37 ± 0.01 Å.

From temperature-dependent magnetic susceptibility measurements (2−290 K), it has been established that $[Cu^{II}(L^3)]$ is paramagnetic and $[Zn(L^3)]$ is diamagnetic. The copper complex exhibits a temperature-independent magnetic moment of 1.8 μ_B (g = 2.21) typical for a copper(II) ion (d^9).

Reaction of the neutral complexes $[M(L^3)]$ (M = Cu, Zn) in dry CH_2Cl_2 with ferroceniumhexafluorophosphate, $[Fc]PF_6$ (1:1), produces a violet and a green precipitate of $[Cu^{II}(L^4)]PF_6$ and $[Zn^{II}(L^4)]PF_6$, respectively, as depicted in eq 4.

$$[M(L^3)] + [Fc]PF_6 \rightarrow [M(L^4)]PF_6 + Fc \qquad (4)$$

$$M = Cu^{II}, Zn^{II}$$

These complexes are the one-electron oxidized forms of $[M(L^3)]$ (M = Cu, Zn), respectively. The ligand $(L^4)^-$ is a paramagnetic organic radical with an $S = {}^1/_2$ ground state. Temperature-dependent magnetic susceptibility measurements (3−290 K) reveal a temperature-independent magnetic moment of 1.8 μ_B (g = 2.002) for $[Zn(L^4)]PF_6$ containing a diamagnetic Zn^{II} ion

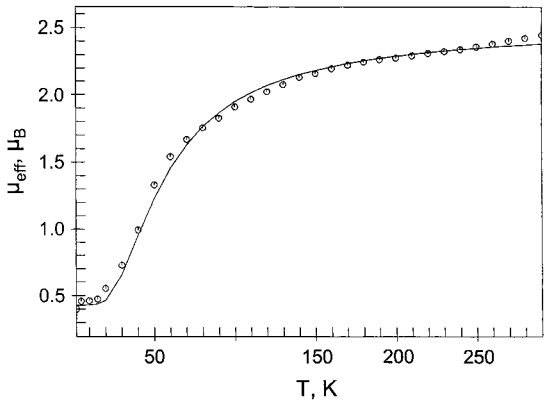

Figure 2. Temperature dependence of the magnetic moment of solid $[Cu^{II}(L^4)]PF_6$. The solid line represents a fit using parameters described in the text.

and a paramagnetic $(L^4)^-$ ligand. In contrast, $[Cu^{II}(L^4)]PF_6$ is a compound containing a $Cu^{II}(d^9)$ ion *and* a coordinated radical $(L^4)^-$. Therefore, spin coupling is expected. Figure 2 shows the temperature dependence of the effective magnetic moment of solid $[Cu^{II}(L^4)]PF_6$. At 290 K, the effective magnetic moment is 2.4 μ_B, which decreases with decreasing temperature to 0.45 μ_B at 5 K. We have modeled this temperature dependence by using the usual spin Hamiltonian $H = -2JS_{L^4} \cdot S_{Cu}$, where J is the coupling constant and $S_{L^4} = S_{Cu} = {}^1/_2$, with the parameters $J = -48.5$ cm^{-1}, $g_{L^4} = 2.002$, and $g_{Cu} = 2.23$ and 6% of a paramagnetic impurity ($S = {}^1/_2$) corresponding to the reduced form $[Cu^{II}(L^3)]$. An antiferromagnetic coupling in $[Cu^{II}(L^4)]PF_6$ generates an $S = 0$ ground state—but see the EPR results below. This coupling is predominantly inter- rather than intramolecular in nature, and the coupling constant J does not represent intramolecular spin exchange coupling between the organic radical and the Cu^{II} ion.

When a blue solution of $[Zn(L^3)]$ in dry CH_2Cl_2 was irradiated at 20 °C with UV light (Hg immersion lamp), a color change to bright red was observed within 1.5 h. Addition of [TBA]ClO_4 initiated the precipitation of diamagnetic red $[Zn^{II}(L^5)](ClO_4)_2$. Extraction of the residual solution with water allows the quantitative determination of generated chloride ions according to eq 5. 1,2-Dichloroethane has been determined as the

$$[Zn^{II}(L^3)] + 2CH_2Cl_2 \xrightarrow{h\nu} [Zn^{II}(L^5)]^{2+} + ClH_2CCH_2Cl + 2Cl^- \quad (5)$$

reduction product by GC/MS and ^{1}H NMR spectroscopy. Thus, the solvent CH_2Cl_2 is the effective scavenger of the photochemically generated electrons. Complex $[Zn(L^5)](ClO_4)_2$ represents the two-electron oxidized form of $[Zn(L^3)]$. Similarly, $[Cu^{II}(L^3)]$ is also photosensitive, but we have only been able to isolate a solid material consisting of a mixture of $[Cu^{II}(L^4)]X$ and $[Cu^{II}(L^5)]X_2$, where X is PF_6^- or ClO_4^-. A pure sample of red $[Cu^{II}(L^5)](ClO_4)_2$ has been obtained from the reaction of $[Cu^{II}(L^3)]$ with 2 equiv of the strong one-electron oxidant $[Ni^{III}(tacn)_2](ClO_4)_3$[9] in CH_2Cl_2 solution, where tacn is the ligand 1,4,7-triazacyclononane (eq 6). From temperature-dependent

$$[Cu^{II}(L^3)] + 2[Ni^{III}(tacn)_2](ClO_4)_3 \rightarrow [Cu^{II}(L^5)](ClO_4)_2 + 2[Ni^{II}(tacn)_2](ClO_4)_2 \quad (6)$$

susceptibility measurements in the range 3−290 K, a temperature-independent magnetic moment of 1.88 μ_B ($g = 2.18$) has been established for $[Cu^{II}(L^5)](ClO_4)_2$, indicative of a paramagnetic Cu^{II} ion and diamagnetic L^5. Complex $[Zn(L^5)](ClO_4)_2$ is diamagnetic.

The reaction of the ligand H_4L^1 with $Cu^{II}(ClO_4)_2 \cdot 6H_2O$ or $Zn(ClO_4)_2 \cdot 6H_2O$ (1:1) in dry methanol under an argon atmosphere with 2 equiv of NEt_3 yielded brown microcrystals of $[Cu^{II}(H_2L^1)]^0$ or $[Zn^{II}(H_2L^1)]^0$. Both compounds are air sensitive and must be kept under anaerobic conditions. $[Cu^{II}(H_2L^1)]^0$ is paramagnetic, with an effective magnetic moment of 1.69−1.82 μ_B in the range 20−300 K and $g = 2.21$, whereas $[Zn^{II}(H_2L^1)]^0$ is diamagnetic.

The solution structure of $[Zn^{II}(H_2L^1)]$ in dry $CDCl_3$ has been established by NMR spectroscopy. The ^{1}H NMR spectrum displays two singlets for the four *tert*-butyl and three signals in the aromatic region, with intensities 2H:4H:2H. In addition, one broad signal at 5.2 ppm (2H) is observed. The relative intensity of a broad signal at 5.9 ppm (<1 H) is sample dependent and may correspond to a small impurity of $[Zn(H_2L^1)(H_2O)]$. In a 2D ^{1}H−^{15}N hetero-multiquantum coherence (HMQC) spectrum, the signal at $\delta = 5.2$ shows a cross-peak to a nitrogen at $\delta = -315$ ppm. The delay for polarization transfer between ^{1}H and ^{15}N was set to 5.5 ms, which corresponds to a coupling constant of 90 Hz. The presence of this signal proves that this proton is bound to a nitrogen and not a phenol oxygen. Therefore, we propose the following structure for the two $[M^{II}(H_2L^1)]$ complexes. We have not found evidence for species containing coordinated phenol ligands in solution.

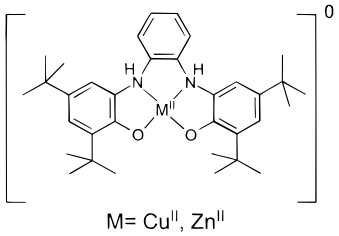

M= Cu^{II}, Zn^{II}

(i) Electro- and Spectroelectrochemistry. Figure 3 displays the cyclic voltammograms of $[M(L^3)]$ (M = Cu, Zn) in CH_2Cl_2 containing 0.10 M tetra-*n*-butylammonium hexafluorophosphate as supporting electrolyte. Both CVs are quite similar: they display two successive one-electron reduction and two successive one-electron oxidation waves, which we assign as shown in Scheme 3. In each case, the four redox waves involve ligand- rather than metal-centered one-electron processes. Thus, in the potential range from +1.5 to −2.0 V vs Fc^+/Fc, the copper(II) ion is not reduced to Cu^I, since the CV of the corresponding zinc species recorded in the same potential range is nearly identical.

Controlled potential coulometry established that the four redox waves are one-electron processes and that all five redox states of $[Zn(L^3)]$ are stable on the time scale of such an experiment at ambient temperature (20 min), whereas for $[Cu^{II}(L^3)]$ the most reduced form, $[Cu^{II}(L^1)]^{2-}$, is not stable in solution.

Figures 4 and 5 display the electronic spectra of the parent species $[M(L^3)]$ (M = Cu and Zn, respectively) and their electrochemically oxidized and reduced forms. The spectral changes within each series of one-electron-transfer steps are quite dramatic. The color of a complex in a given oxidation level is indicated in Scheme 3. Table 2 gives the electronic spectra of all electrochemically generated species, and Figure 6 displays the spectra of $[Cu^{II}(H_2L^1)]$ and $[Zn^{II}(H_2L^1)]$ in CH_2Cl_2 solution.

(9) Wieghardt, K.; Walz, W.; Nuber, B.; Weiss, J.; Ozarowski, A.; Stratemeier, H.; Reinen, D. *Inorg. Chem.* **1986**, *25*, 1650.

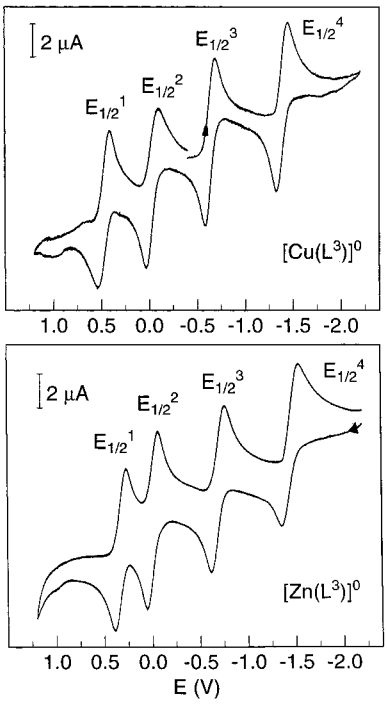

Figure 3. Cyclic voltammograms of $[Cu^{II}(L^3)]$ (top) and $[Zn(L^3)]$ (bottom) in CH_2Cl_2 at 298 K (0.10 M $[TBA]PF_6$ supporting electrolyte; glassy carbon working electrode; scan rate 100 mV s^{-1}). The potentials are given in volts vs the Fc^+/Fc couple.

Scheme 3. Summary of the Electrochemistry of $[M(L^3)]$ (M = Cu, Zn) in CH_2Cl_2 (0.10 M $[TBA]PF_6$)[a]

	M= Cu^{II}	M= Zn^{II}
$[M^{II}(L^5)]^{2+}$	red (S=½)	red (S=0)
-e ⇅ +e $E^1_{½}$	0.41	0.37
$[M^{II}(L^4)]^{+}$	violet (S=0)	green (S=½)
-e ⇅ +e $E^2_{½}$	-0.06	0.03
$[M^{II}(L^3)]^{0}$	green (S=½)	blue (S=0)
-e ⇅ +e $E^3_{½}$	-0.66	-0.64
$[M^{II}(L^2)]^{-}$	blue (S=0)	green (S=½)
-e ⇅ +e $E^4_{½}$	-1.42	-1.29
$[M^{II}(L^1)]^{2-}$	yellow (S=½)	colorless (S=0)

[a] Redox potentials are referenced in volts vs the ferrocenium/ferrocene couple; the indicated colors of solutions are observed after coulometry at the appropriate fixed potential.

(ii) EPR Spectroscopy. X-band EPR spectra of $[Zn^{II}(L^4)]^+$ and $[Zn^{II}(L^2)]^-$ in CH_2Cl_2 solution (0.10 M $[TBA]PF_6$), generated electrochemically from $[Zn(L^3)]$ by one-electron oxidation and reduction, respectively, have been recorded at 298 K. The spectra and their simulations are displayed in Figure 7. Both species exhibit typical $S = {}^1/_2$ signals with hyperfine structure. The spectrum of the monoanion $[Zn^{II}(L^2)]^-$ displays a signal at $g = 2.0045$ with hyperfine splitting from only one nitrogen atom and one proton, in excellent agreement with the resonance structure for an iminosemiquinone moiety in $(L^2)^{3-}$ (Scheme 2). In contrast, the spectrum of $[Zn^{II}(L^4)]^+$ shows a signal at $g = 2.0045$ with hyperfine splittings from two nitrogen atoms and four different protons, indicating delocalization of the unpaired electron over the iminoquinone and both phenolate rings in $(L^4)^-$. These spectra prove that the redox chemistry of $[Zn^{II}(L^3)]$ is ligand-based. Both $[Zn(L^5)]^{2+}$ and $[Zn(L^1)]^{2-}$ are diamagnetic species.

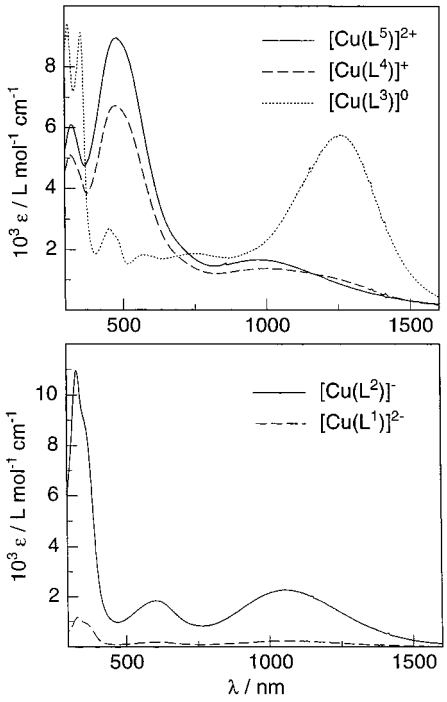

Figure 4. Electronic spectra of electrochemically generated oxidized (top) and reduced (bottom) forms of $[Cu^{II}(L^3)]$ in CH_2Cl_2 (0.10 M $[TBA]PF_6$).

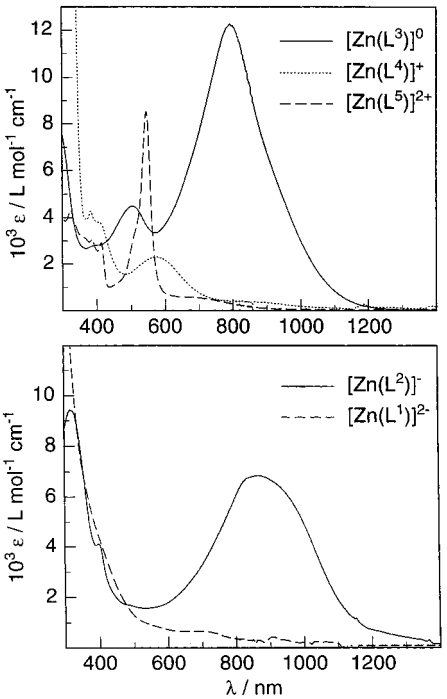

Figure 5. Electronic spectra of electrochemically generated oxidized (top) and reduced (bottom) forms of $[Zn(L^3)]$ in CH_2Cl_2 (0.10 M $[TBA]PF_6$).

Since the redox potentials $E_{1/2}{}^{1-4}$ (Scheme 3) for the Zn^{II} and Cu^{II} complexes are very similar, we conclude that the redox chemistry of $[Cu^{II}(L^3)]$ is also ligand-based, giving rise to paramagnetic $S_{Cu} = {}^1/_2$ ground states in $[Cu^{II}(L^3)]$ and $[Cu^{II}(L^5)](ClO_4)_2$ and $[Cu^{II}(L^1)]^{2-}$ or $[Cu^{II}(L^1H_2)]$, but $S_t = 0$ ground states for $[Cu^{II}(L^4)]PF_6$ and $[Cu(L^2)]^-$. The latter are attained

Table 2. Electronic Spectra of Complexes (300−1600 nm, CH_2Cl_2)

	λ_{max}, nm (ϵ, L mol^{-1} cm^{-1})
$[Cu^{II}(L^5)](ClO_4)_2$	311 (1.0×10^4), 350 sh, 455 (9.1×10^3), 976 (1.25×10^3)
$[Cu^{II}(L^4)]PF_6$	320 (5.1×10^3), 478 (6.4×10^3), 981 (1.2×10^3)
$[Cu^{II}(L^3)]$	315 (9.0×10^3), 356 (8.5×10^3), 453 (2.5×10^3), 483 sh (2.2×10^3), 575 (1.7×10^3), 747 (1.8×10^3), 1256 (5.6×10^3)
$[Cu^{II}(L^2)]^-$ [a]	330 (10.8×10^3), 400 sh, 607 (1.9×10^3), 1073 (2.5×10^3)
$[Cu^{II}(L^1)]^{2-}$	334 (1.2×10^3), 369 (855), 600 (170), 1053 (214)
$[Cu^{II}(L^1H_2)]$[b]	453 (2.5×10^3), 540 sh, 700 sh, 906 (2.5×10^3)
$[Cu^{I}(L^1H_2)]^-$ [b]	411 (470), 651 (60)
$[Zn(L^5)](ClO_4)_2$	326 (2.1×10^3), 368 (1.5×10^3), 392 (2.9×10^3), 414 (2.8×10^3), 500 sh, 545 (8.5×10^3), 700 sh
$[Zn(L^4)]PF_6$	385 (4.2×10^3), 411 (3.8×10^3), 578 (2.4×10^3), 810 sh
$[Zn(L^3)]$	405 (3.0×10^3), 506 (4.4×10^3), 798 (12.2×10^3)
$[Zn(L^2)]^-$ [a]	320 (9.0×10^3), 401 (4.0×10^3), 873 (6.8×10^3)
$[Zn(L^1)]^{2-}$ [a]	700 (∼60)
$[Zn(H_2L^1)]$	454 (5.4×10^3), 800 sh

[a] Generated by controlled potential coulometry in CH_2Cl_2 (0.10 M $[TBA]PF_6$). [b] Generated in THF solution; $[L^1H_4] = 10^{-3}$ M, [CuCl] or $[Cu^{II}(ClO_4)_2 \cdot 6H_2O] = 10^{-3}$ M, $[NEt_3] = 2 \times 10^{-3}$ M.

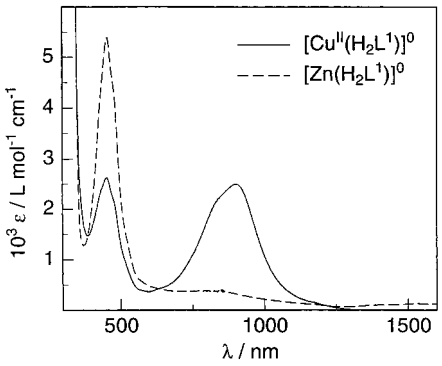

Figure 6. Electronic spectra of $[M^{II}(H_2L^1)]$ (M = Cu^{II}, Zn^{II}) in CH_2Cl_2.

via intramolecular antiferromagnetic coupling of an unpaired electron in a $d_{x^2-y^2}$ orbital and a ligand-based unpaired π-electron.

Complexes$[Cu^{II}(L^3)]$, $[Cu^{II}(L^5)](ClO_4)_2$, and $[Cu^{II}(H_2L^1)]$ display typical EPR spectra of square planar Cu^{II} complexes with copper hyperfine structure. From simulations, we obtained the parameters given in Table 3. The spectra and simulations are shown in Figures S1, S5, and S2 in the Supporting Information, respectively.

Interestingly, $[Cu(L^2)]^-$ in CH_2Cl_2 is EPR silent at low temperatures (<70 K) but shows a broad unresolved spectrum of an $S = 1$ system at temperatures >80 K. We take this as experimental evidence that this species has a diamagnetic ground state where the ligand radical $(L^2)^{3-}$ ($S = {}^1/_2$) is antiferromagnetically coupled to a Cu^{II} ion ($S = {}^1/_2$).

Similarly, the spectrum of $[Cu^{II}(L^4)]PF_6$ in CH_2Cl_2 shows signals at $g_{eff} \approx 2.0$ and a typical half-field signal of an $S = 1$ system at $g_{eff} \approx 4.0$ at 50 K (Figure S3, Supporting Information). The latter signal disappears upon decreasing the temperature. From its temperature dependence, an antiferromagnetic coupling constant of $J = -7 \pm 3$ cm^{-1} was calculated (Figure S4, Supporting Information) by using the spin Hamiltonian $H = -2JS_{rad} \cdot S_{Cu}$ ($S_{rad} = S_{Cu} = {}^1/_2$). This intramolecular coupling of -7 cm^{-1} in solution is significantly smaller than the value obtained from temperature-dependent magnetic susceptibility measurements on a solid sample of $[Cu^{II}(L^4)]PF_6$ (see above).

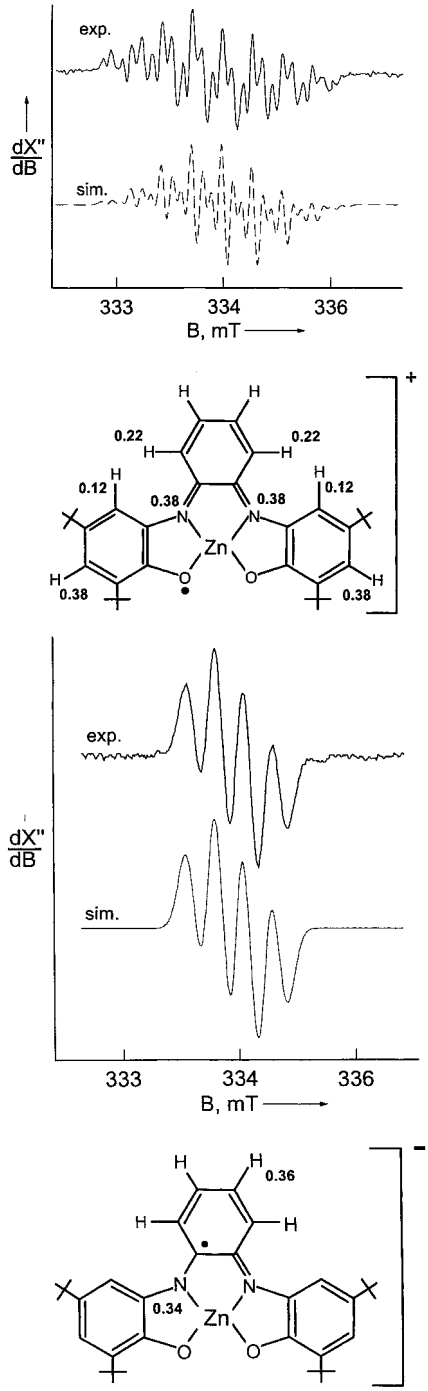

Figure 7. X-band EPR spectra of electrochemically generated $[Zn(L^4)]^+$ (top) and $[Zn(L^2)]^-$ (bottom) in CH_2Cl_2 (0.10 M $[TBA]PF_6$) at 298 K and their simulations. Experimental conditions: [complex], $\sim 10^{-4}$ M; frequency, 9.4501 GHz; microwave power, 10 mW; modulation amplitude, 0.05 mT; gain, 3200. The hyperfine coupling constants are given in millitesla.

Table 3. EPR Spectra of Cu^{II} Complexes in CH_2Cl_2 Solution

complex	T, K	g_x	g_y	g_z	$A_x = A_y$, $\times 10^4$ cm^{-1}	A_z, $\times 10^4$ cm^{-1}
$[Cu^{II}(H_2L^1)]$	10	2.059	2.067	2.278	11	183
$[Cu^{II}(L^3)]^0$	10	2.062	2.062	2.278	10	155
$[Cu^{II}(L^5)](ClO_4)_2$	4	2.044	2.076	2.224	32	156

This indicates that, in addition to a relatively small intramolecular exchange coupling, there also exists a relatively strong intermolecular interaction in the solid state.

Single Turnover of $[Cu^{II}(L^4)]^+$ and $[Zn^{II}(L^4)]^+$ with Primary Alcohols. When a solution of $[Cu^{II}(L^4)]PF_6$ and NEt_3 (1:2) in dry CH_2Cl_2 was added to an excess of a primary alcohol such as methanol, ethanol, or benzyl alcohol under anaerobic conditions (Ar) at 22 ± 1 °C, the original violet color changed to deep blue within minutes. The final UV/vis spectrum of this solution corresponds to that of $[Cu^{II}(L^2)]^-$ generated electrochemically from $[Cu^{II}(L^3)]$ in CH_2Cl_2. ^1H NMR/GC analysis of the resulting solution indicates the formation of formaldehyde, acetaldehyde, and benzaldehyde, respectively. Spectrophotometric quantitative determination of these aldehydes[10] indicates a stoichiometry as in eq 7 with >95% yield of aldehyde and $[Cu^{II}(L^2)]^-$, respectively.

$$R{-}CH_2OH + [Cu^{II}(L^4)]^+ \xrightarrow[-2[HNEt_3]^+]{+2NEt_3} R{-}CHO + [Cu^{II}(L^2)]^- \quad (7)$$

$$R = H, CH_3, \text{phenyl}$$

Thus, complex $[Cu^{II}(L^4)]^+$ is capable of oxidizing primary alcohols to the corresponding aldehyde and forming the two-electron reduced form $[Cu^{II}(L^2)]^-$. No reaction was observed when using secondary alcohols (2-propanol or diphenylcarbinol) using the same conditions.

Similarly, the zinc-containing monocationic complex $[Zn(L^4)]^+$ undergoes the same reaction (eq 8) as was established by following the reaction spectrophotometrically and with GC product analysis.

$$R{-}CH_2OH + [Zn^{II}(L^4)]^+ \xrightarrow[-2[HNEt_3]^+]{+2NEt_3} R{-}CHO + [Zn^{II}(L^2)]^- \quad (8)$$

$$R = H, CH_3, \text{phenyl}$$

The final UV/vis spectrum of the solution is identical to that of electrochemically generated $[Zn(L^2)]^-$ (from $[Zn(L^3)]^0$ via coulometric one-electron reduction).

Interestingly, neither $[Cu^{II}(L^3)]$ nor $[Zn^{II}(L^3)]$ reacts with the above alcohols. Both species have not been detected as intermediates or products in the reaction of $[Cu^{II}(L^4)]^+$ and $[Zn(L^4)]^+$ with primary alcohols. In contrast, upon mixing of two aliquots of CH_2Cl_2 solutions containing only electrochemically generated (a) $[Cu^{II}(L^4)]^+$ (or $[Zn^{II}(L^4)]^+$) and (b) $[Cu^{II}(L^2)]^-$ (or $[Zn^{II}(L^2)]^-$), the spectrum of $[Cu^{II}(L^3)]^0$ (or $[Zn^{II}(L^3)]^0$) is generated within mixing time according to eq 9 via comproportionation.

$$[M^{II}(L^4)]^+ + [M^{II}(L^2)]^- \rightarrow 2[M^{II}(L^3)]^0 \quad (9)$$

$$M^{II} = Cu \text{ or } Zn$$

We take the fact that the $[M(L^3)]$ species are not observed in the slow reduction of $[M(L^4)]^+$ by an alcohol as an indication that, under our experimental conditions—using a large excess of alcohol over the $[M(L^4)]^+$ species—a five-coordinate species, $[M(HL^4)(OR)]^+$, prevails which does not undergo a one-electron reduction by the product $[M(L^2)]^-$. We have tested this assumption by using the following experiment. The absorption coefficients of a solution containing $[Cu^{II}(L^4)]^+$ and, independently, of solutions containing $[Cu^{II}(L^3)]$ and of $[Cu(L^2)]^-$ in methanol at 450 nm were measured. Each of the three solutions contained the same overall copper(II) concentration. We then prepared a fourth methanol solution in which we combined two aliquots of solutions containing (a) $[Cu^{II}(L^4)]^+$ and (b) $[Cu^{II}(L^2)]^-$, and we measured the absorbance at 450 nm. If the latter solution contains equal amounts of unreacted $[Cu(L^4)]^+$ and $[Cu(L^2)]^-$, then the observed molar extinction coefficient, ϵ_{450}, is expected to be 3.6×10^3 L mol^{-1} cm^{-1}; if, on the other hand, comproportionation has taken place, ϵ_{450} is expected to be 1.6×10^3 L mol^{-1} cm^{-1}. The experimental value, $\epsilon_{450} = 3.5 \times 10^3$ L mol^{-1} cm^{-1}, confirms that, in methanol solution, no comproportionation between $[Cu(L^4)]^+$ and $[Cu(L^2)]^-$ occurs.

Table 4. Kinetic Data of Anaerobic Single-Turnover Reactions at 22 ± 1 °C

oxidant	reductant	condns[a]	K, M^{-1}	k, s^{-1}	K_H/K_D	k_H/k_D
$[Cu^{II}(L^4)]^+$	CH_3OH	1	79 ± 15	$(1.2 \pm 0.6) \times 10^{-5}$	1.01	54
$[Cu^{II}(L^4)]^+$	CD_3OH	1	78 ± 5	$(2.9 \pm 0.05) \times 10^{-7}$		
$[Cu^{II}(L^4)]^+$	CH_3CH_2OH	2	20 ± 6	$(2.0 \pm 0.3) \times 10^{-5}$	0.95	14
$[Cu^{II}(L^4)]^+$	CH_3CD_2OH	2	21 ± 2	$(1.4 \pm 0.6) \times 10^{-6}$		
$[Zn(L^4)]^+$	CH_3CH_2OH	3	12 ± 3	$(1.6 \pm 0.3) \times 10^{-6}$	1.33	15
$[Zn(L^4)]^+$	CH_3CD_2OH	3	9 ± 2	$(1.1 \pm 0.2) \times 10^{-7}$		

[a] Reaction conditions: (1) solvent CH_2Cl_2, $[Cu^{II}(L^4)^+] = 3.5 \times 10^{-4}$ M, [methanol] = 2.5×10^{-3}–2.0×10^{-2} M, $[NEt_3] = 7.1 \times 10^{-4}$ M; (2) solvent CH_2Cl_2 containing 0.10 M $[TBA]PF_6$, electrochemically generated $[Cu(L^4)]^+$ (from $[Cu(L^3)]$, 3.5×10^{-4} M), [ethanol] = 8.0×10^{-3}–8.0×10^{-2} M, $[NEt_3] = 7.1 \times 10^{-4}$ M; (3) solvent CH_2Cl_2, $[Zn(L^4)^+] = 3.5 \times 10^{-4}$ M, [ethanol] = 5×10^{-3}–0.25 M, $[NEt_3] = 7.1 \times 10^{-4}$ M. All reactions were run under an Ar blanketing atmosphere.

The kinetics of the reactions of $[M(L^4)]^+$ (M = Cu, Zn) with methanol and ethanol (eqs 7 and 8, respectively) have been measured spectrophotometrically in CH_2Cl_2 solution at 22 ± 1 °C under an argon blanketing atmosphere. Two equivalents of NEt_3 (7.1×10^{-4} M) had been added in each experiment as a proton scavenger. The spectral changes at 454 nm for **2** and at 578 nm for **5** have been measured as a function of time using pseudo-first-order conditions with an excess alcohol (0.005–0.25 M) and [complex] = 3.5×10^{-4} M. First-order rate constants, k_{obs}, plotted vs the alcohol concentration displayed saturation behavior as in eq 10. Numerical values for the

$$k_{obs} = \frac{kK[\text{alcohol}]}{1 + K[\text{alcohol}]} \quad (10)$$

equilibrium constants K (in M^{-1}) and the rate constant k (in s^{-1}) were evaluated from a least-squares fit of the data to eq 10 and are summarized in Table 4.

The simplest mechanism in accord with the above kinetic data involves reversible binding of one molecule of alcohol to the complex $[M(L^4)]^+$ (M = Cu, Zn) and irreversible oxidation of it in the rate-determining step (eqs 11 and 12).

$$[M(L^4)]^+ + RCH_2OH \overset{K}{\rightleftharpoons} [M(L^4)(OCH_2R)] + H^+ \quad (11)$$

$$[M(L^4)(OR)] \xrightarrow{k} [M(L^2)]^- + RCHO + H^+ \quad (12)$$

The kinetics of the same reactions using the selectively deuterated substrates CD_3OH and CH_3CD_2OH have also been measured under the same reaction conditions as for the unlabeled alcohols. Significantly, the ratio K_H/K_D is in the range 0.95–1.33, which implies that the binding of the substrate does not

(10) Kakác, B.; Vejdelek, Z. J. *Handbuch der photometrischen Analyse organischer Verbindungen*; Verlag Chemie, Weinheim, 1974; Vol. 1, pp 257 and 259.

Scheme 4

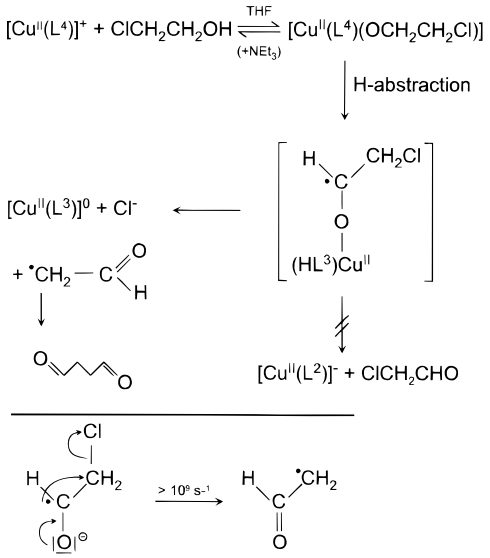

exhibit a marked isotope effect. In contrast, the k_H/k_D ratios of 54 for the reaction of methanol with $[Cu^{II}(L^4)]^+$ and of 14 ± 1 for the reactions of $[M(L^4)]^+$ (M = Cu, Zn) with ethanol indicate a significant large kinetic isotope effect (KIE). We take this as clear evidence that H-abstraction from the α-carbon atom of the coordinated alcohol is the rate-determining step. The resulting coordinated ketyl radical anion is known to be a strong one-electron reductant[11] which is converted to the aldehyde via an intramolecular one-electron-transfer step. In the present cases, this intramolecular electron-transfer step reduces the ligand from the $(L^3)^{2-}$ to the $(L^2)^{3-}$ oxidation level.

Interestingly, the stoichiometric reaction of $[Cu^{II}(L^4)](PF_6)$ (3.1×10^{-4} M) with 2-chloroethanol (3.1×10^{-3} M) under an argon atmosphere in the presence of triethylamine (6.3×10^{-4} M) in dry THF at 22 °C produces within 20 min quantitatively the *one*-electron reduced complex $[Cu^{II}(L^3)]$, succinic dialdehyde (95%), and free chloride ions (95%) according to the reaction sequence shown in Scheme 4. In contrast, as shown above, the same reaction with the substrate ethanol produces $[Cu^{II}(L^2)]^-$ and acetaldehyde. It is well established that the ketyl radical anion $^-O-\dot{C}H-CH_2Cl$ rearranges intramolecularly very rapidly ($k > 10^9$ s^{-1}), with formation of free chloride ions and the C-centered radical $\dot{C}H_2CHO$,[3a,12] which is a poor ligand and dimerizes in solution with formation of succinic dialdehyde. We have not been able to identify any chloroacetaldehyde (<1%) (or $[Cu(L^2)]^-$) as product in the above reaction. This proves that H atom abstraction is the rate-determining step of alcohol oxidation by $[M(L^4)]^+$ (M = Cu^{II}, Zn^{II}) and not hydride transfer, which would necessitate the products chloroacetaldehyde and $[Cu^{II}(L^2)]^-$. Furthermore, the quantitative formation of succinic dialdehyde and chloride ions indicates that the alternative intramolecular electron transfer from the coordinated ketyl radical anion to the $Cu^{II}(L^3)$ unit is significantly slower (at least 2 orders of magnitude) than the above intramolecular rearrangement of the radical with expulsion of Cl^- (i.e., $k_{et} \ll k_{rearr} = 10^9$ s^{-1}). The reaction of $[Zn(L^4)]PF_6$ with 2-chloroethanol also yields quantitatively one-electron reduced $[Zn(L^3)]$, succinic dialdehyde, and chloride ions.

(11) Wang, W.-F.; Schuchmann, M. N.; Bachler, V.; Schuchmann, H.-P.; von Sonntag, C. *J. Phys. Chem.* **1996**, *100*, 15843 and references therein.

(12) (a) Tanner, D. D.; Chen, J. J.; Chen, L.; Luelo, C. *J. Am. Chem. Soc.* **1991**, *113*, 8074. (b) Tanner, D. D.; Yang, C.-M. *J. Org. Chem.* **1993**, *58*, 5907. (c) Tanner, D. D.; Xie, G.-J.; Hooz, J.; Yang, C.-M. *J. Org. Chem.* **1993**, *58*, 7138.

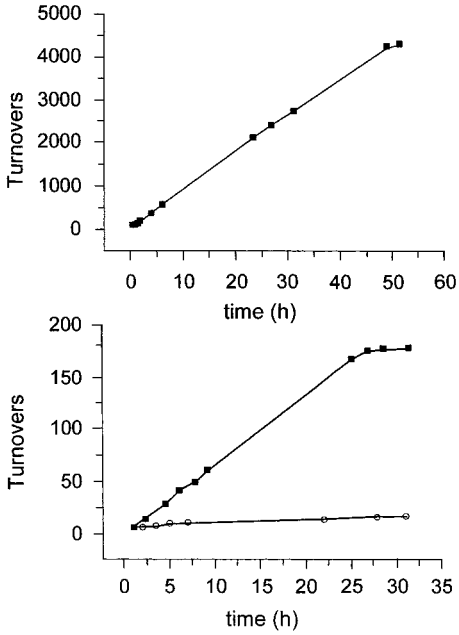

Figure 8. Plot of the turnover versus time of the catalyses at 22 ± 1 °C in THF. Top: $[Cu(L^4)] = 2.5 \times 10^{-4}$ M, $[NEt_3] = 5.0 \times 10^{-4}$ M, [ethanol] = 2.5 M in the presence of air (1 bar). Bottom: $[Zn(L^4)^+] = 2.5 \times 10^{-4}$ M, $[NEt_3] = 5.0 \times 10^{-4}$ M, [ethanol] = 2.5 M (■); and $[Zn(L^3)] = 2.5 \times 10^{-4}$ M, $[NEt_3] = 5.0 \times 10^{-4}$ M, [ethanol] = 2.5 M (○) in the presence of air. The turnover is defined as the ratio [acetaldehyde]/[catalyst] or (indistinguishably) $[H_2O_2]$/[catalyst] at a given point in time.

Reaction of $[Cu^{II}(L^2)]^-$ and $[Zn(L^2)]^-$ with O_2. When a solution containing electrochemically generated $[Cu^{II}(L^2)]^-$ (3.5×10^{-4} M) and acetic acid (7.1×10^{-4} M) in CH_2Cl_2 (0.1 M [TBA]PF_6) was exposed to dioxygen, the color changed within 2−3 min from blue to violet. The electronic absorption spectrum of this solution corresponds to that of $[Cu^{II}(L^4)]^+$ in CH_2Cl_2 (0.1 M [TBA]PF_6). In addition, 1 equiv of H_2O_2 has been detected. Thus, the rapid reaction of $[Cu^{II}(L^2)]^-$ with O_2 quantitatively yields H_2O_2 and $[Cu(L^4)]^+$ (eq 13) in the presence of protons (acetic acid). Similar experiments with $[Zn^{II}(L^2)]^-$

$$[Cu^{II}(L^2)]^- + O_2 + 2H^+ \rightarrow [Cu^{II}(L^4)]^+ + H_2O_2 \quad (13)$$

and O_2 produced also H_2O_2 and $[Zn^{II}(L^4)]^+$ (eq 14). Reactions

$$[Zn^{II}(L^2)]^- + O_2 + 2H^+ \rightarrow [Zn^{II}(L^4)]^+ + H_2O_2 \quad (14)$$

13 and 14 represent formally a two-electron oxidation of the ligand $(L^2)^{3-}$ to $(L^4)^-$.

Homogeneous Catalysis. The stoichiometric reactions equations (eqs 7, 8 and eqs 13, 14) taken together immediately imply that, in principle, the oxidation of primary alcohols by dioxygen should be catalyzed by the complexes $[M(L^4)]^+$ (M = Cu, Zn). This is, indeed, the case.

Figure 8a shows the result of an experiment where the formation of acetaldehyde and H_2O_2 from ethanol (2.5 M) and air (1 bar) in THF in the presence of the catalyst $[Cu(L^4)]^+$ (2.5×10^{-4} M) was monitored at 22 °C as a function of time. The catalysis stopped after ∼45 h. For the first 40 h, the turnover increases linearly with time, where the turnover is defined as the ratio [aldehyde]/[catalyst] or (indistinguishably) $[H_2O_2]$/[catalyst] at a given point in time. During this time, the color of the solution is greenish, and its electronic spectrum resembles that of $[Cu(L^4)]^+$. After ∼40 h, the color changed to yellow, at which point the reaction stopped rather abruptly; ∼50%

Table 5. Kinetic Data of Catalytic Reactions at 22 + 1 °C

catalyst	alcohol	condns[a]	K, M^{-1}	k, s^{-1}	K_H/K_D	k_H/k_D
$[Cu(L^4)]^+$	CH_3OH	1	12 ± 2	$(5.0 \pm 0.3) \times 10^{-6}$	0.92	36
	CD_3OH	1	13 ± 3	$(1.4 \pm 0.2) \times 10^{-7}$		
$[Cu(L^4)]^+$	CH_3CH_2OH	1	0.5 ± 0.1	$(1.6 \pm 0.09) \times 10^{-5}$	0.93	10
	CH_3CD_2OH	1	0.54 ± 0.09	$(1.6 \pm 0.2) \times 10^{-6}$		
$[Zn(L^4)]^+$	CH_3CH_2OH	2	0.6 ± 0.2	$(6.8 \pm 1.3) \times 10^{-7}$	1.5	11
	CH_3CD_2OH	2	0.4 ± 0.1	$(6.0 \pm 0.1) \times 10^{-8}$		

[a] Reaction conditions: (1) $[H_4L^1] = 2.5 \times 10^{-4}$ M, $[Cu^ICl] = 2.5 \times 10^{-4}$ M, $[NEt_3] = 10^{-3}$ M in tetrahydrofuran, [alcohol] = 0.01−2.5 M, stirred under 1 bar of air at 22 ± 1 °C; (2) as in (1) but using $Zn(ClO_4)_2 \cdot 6H_2O$ instead of Cu^ICl.

conversion of the substrate ethanol had been achieved. In a similar experiment, which is shown in Figure 8b, using identical reaction conditions except that $[Zn(L^4)]^+$ was used as catalyst (2.5×10^{-4} M), again a linear increase of turnovers with time is observed but only for ~25 h, after which time the reaction stopped. Within 25 h, only 170 turnovers were achieved; the conversion was ~2%. Thus, the zinc is a far less effective and stable catalyst than its copper analogue. When the same experiments as described above were performed using $[Cu^{II}(L^3)]$ and $[Zn(L^3)]$ as catalyst, a pronounced kinetic lag phase was observed; both species are not the catalytically competent forms of the complexes.

We have measured the kinetics of the catalyses under turnover conditions by using the initial rate method, where the concentration of the respective catalyst was varied in the range 2.5×10^{-4}−2.5×10^{-3} M and that of the alcohol (methanol and ethanol) in the range 0.01−2.5 M and $[NEt_3] = 2$[catalyst]. The formation of the aldehyde and, independently, of H_2O_2 was monitored spectrophotometrically as a function of time (see Experimental Section for details). The rate of formation of both products is identical. This implies that the catalysts do not catalyze the disproportionation of H_2O_2. A rate law (eq 15) was thus established.

$$\text{rate} = \left(\frac{kK[\text{alcohol}]}{1 + K[\text{alcohol}]}\right)[\text{catalyst}] \qquad (15)$$

We have also briefly studied the effect of $[NEt_3]$ on the catalysis.[7] In a series of experiments with [ethanol] = 0.125 M = constant and $[Cu(L^4)^+] = 2.5 \times 10^{-4}$ M = constant and variation of $[NEt_3] = 5.0 \times 10^{-4}$−$2.0 \times 10^{-3}$ M, it was found that, when the ratio $[NEt_3]/[Cu(L^4)^+] > 4$, the catalysis is effectively inhibited, and at a ratio ~5 catalysis does not proceed. This is a clear indication that the base triethylamine is a competitive inhibitor which binds more effectively to $[Cu(L^4)]^+$ than the substrate alcohol. We also note that acetonitrile is a very effective inhibitor.

Table 5 summarizes numerical values of k and K obtained from a least-squares fit the kinetic data to eq 15. We have also investigated the reaction with the selectively deuterium labeled substrates CD_3OH and CH_3CD_2OH.

The observed first-order dependence of the rate on the concentration of $[Cu(L^4)]PF_6$ or $[Zn(L^4)]PF_6$ clearly indicates that the monomeric cations represent the catalytically active forms and not a dinuclear species, such as complex B in Chart 1.[7] The observed saturation kinetics for the catalyses allows one to determine the binding constants of the substrate to the catalyst.

Interestingly, the alcohol binding constants, K_H and K_D, measured under turnover conditions are of the same order of magnitude as those determined for the stoichiometric reactions (eqs 7, 8). The difference is mainly due to the fact that the stoichiometric reactions were run in CH_2Cl_2 (a noncoordinating solvent), whereas the catalysis was performed in THF (weakly coordinating). The ratio K_H/K_D is in the range 0.92−1.5, indicating the lack of a significant isotope effect. In contrast, the ratio k_H/k_D under turnover conditions is 36 and 10 for methanol and ethanol substrates, respectively, indicating a significant KIE. The numerical values for k_H^{cat} and k_D^{cat} are very similar to those found for the stoichiometric reactions (k_H, k_D). This implies that reoxidation of the reduced catalysts by oxygen is fast compared to the oxidation of alcohols.

The catalysts can also be assembled in situ from solutions of the ligand H_4L^1 and CuCl (1:1) or $Zn^{II}(ClO_4)_2 \cdot 6H_2O$ in THF under anaerobic conditions. Upon exposure to air, the catalytically active forms $[Cu(L^4)]^+$ and $[Zn(L^4)]^+$ are generated with formation of 2 and 1.5 equiv of H_2O_2, respectively, as depicted in eqs 16 and 17.

$$H_4L^1 + CuCl \rightarrow [Cu^I(L^1H_4)]^+ \xrightarrow[-H_2O_2]{+O_2} \rightarrow [Cu^{II}(L^2H_2)]^+ \xrightarrow[-H_2O_2]{+O_2} [Cu^{II}(L^4)]^+ \quad (16)$$

$$H_4L^1 + Zn^{2+} \xrightarrow{+O_2} [Zn^{II}(L^4)]^+ + 1.5H_2O_2 + H^+ \quad (17)$$

The stoichiometry of these reactions has been determined spectrophotometrically ($[Cu^{II}(L^4)]^+$ and $[Zn(L^4)]^+$), and the amount of H_2O_2 produced has been measured spectrophotometrically after its conversion to the peroxotitanyl species (see Experimental Section).

Discussion

In this work, we have presented two mononuclear coordination compounds, $[Cu^{II}(L^4)]PF_6$ and $[Zn(L^4)]PF_6$, which catalyze the selective aerobic oxidation of primary alcohols, including methanol, yielding aldehydes and 1 equiv of H_2O_2. In this sense, they represent functional models for the enzyme GO. Mechanistically, there are subtle differences due to the fact that $[Zn(L^4)]PF_6$, containing a redox-inactive central zinc(II) ion, is also an active catalyst although not quite as efficient as $[Cu^{II}(L^4)]PF_6$.

In Figure 9, we present a minimal mechanistic scheme for the catalysis which is in accord with all the structural and kinetic information assembled above. In the first step, a rapid equilibrium between the catalyst and one molecule of alcohol is established. The alcohol is most probably bound in its anionic alcoholate form, where the proton from the bound alcohol is transferred either to the external base NEt_3 or to the phenolate ligand with formation of a coordinated phenol. Such coordinated phenols have been shown to possess a dissociation constant, pK_a, of ~5−6 in aqueous solution.[4b] Coordination of an alcoholate ligand to $[M(L^4)]^+$ (M = Cu, Zn) results in a five-coordinate, square-base pyramidal intermediate, where the axially bound alcoholate is in *cis*-position relative to the phenoxyl radical ligand.

In this geometrical arrangement, one hydrogen atom of the α-carbon atom of the alcoholate ligand is, in principle, capable of forming a hydrogen bond to the phenoxyl radical ligand, giving rise to a five-membered chelate ring Cu−O···H−C−O.

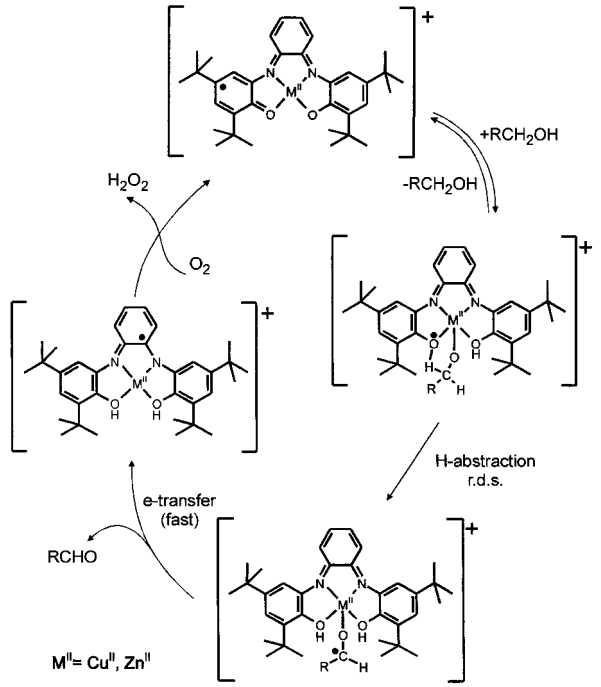

Figure 9. Proposed mechanism for the catalytic oxidation of primary alcohols by dioxygen.

This has been beautifully demonstrated by Tolman et al.,[4a,13] who have shown by X-ray crystallography that the following intramolecular hydrogen-bonding scheme prevails in a mononuclear phenolato(benzyl alcoholato)copper(II) complex. These

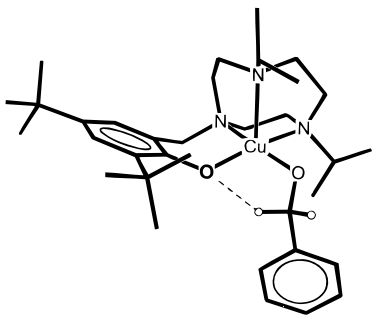

authors have also shown that electrochemical one-electron oxidation of the phenolate to the corresponding phenoxyl triggers an internal redox process whereby benzaldehyde is produced presumably along with Cu^{I}. We suggest that the above five-membered ring resembles the transition state for the H-abstraction reaction in our catalytic systems and in Tolman's model complex. Clearly, this is the rate-determining step in the catalyses with $[M(L^4)]^+$ (M = Cu, Zn), since this intramolecular H-abstraction displays large kinetic isotope effects.

These large KIEs deserve a comment. It is well established that oxidation of primary alcohols by oxo metal complexes such as MnO_4^-,[14] RuO_4,[15] $[(bpy)_2(py)Ru(O)]^{2+}$,[16] $[(trpy)(bpy)Ru(O)]^{2+}$,[17] and, more recently, *trans*-$[Ru^{VI}(trpy)/(O)_2(L)]^{2+}$ (L = H_2O, CH_3CN)[18] display in some instances very large KIEs (up to $k_H/k_D = 61.5$), and, at least for the first two ruthenium complexes,[16,17] a rate-determining hydride transfer from the α-carbon atom of the alcohol to the oxo metal moiety has been proposed. In general, a k_H/k_D of >10 (at 20 °C) has been interpreted as the occurrence of nuclear tunneling,[19] but it is not possible to distinguish between a hydride and a hydrogen atom transfer mechanism (i.e., hetero- vs homolytic C−H scission) by the observed ratio k_H/k_D. As Roecker and Meyer have pointed out,[16] "the experimental facts pertaining to k_H/k_D isotope effects show that they are not amenable to simple interpretation".

It is noteworthy in this respect that Whittaker et al.[3d] have recently reported a detailed study of the KIEs as probes of the mechanism of GO. While steady-state kinetics studies have demonstrated a KIE of 7−8 that was attributed to substrate oxidation (galactose), these authors have used rapid kinetic methods to measure the anaerobic reduction of GO substrate by galactose and found KIEs of 22.5 (4 °C).

Branchaud et al.[3a,20] used simple β-haloethanols as mechanistic probes and demonstrated rapid enzyme inactivation via reduction of the active site to the inactive Cu^{II} form. They concluded that the substrate oxidation step of GO proceeds either "through a short-lived ketyl radical anion intermediate or through a closely related concerted E_2R mechanism with considerable ketyl radical anion character in the transition state".

In this work, the reduction of the radical complex $[Cu^{II}(L^4)]^+$ by the substrates β-chloroethanol on one hand and ethanol on the other, yielding quantitatively $[Cu(L^3)]$ and $[Cu(L^2)]^-$, respectively, and as oxidation products succinic dialdehyde and acetaldehyde, respectively, lends strong support to the notion that a common coordinated ketyl radical anion is formed as an intermediate in the rate-determining step of alcohol oxidation by the catalyst $[Cu^{II}(L^4)]^+$ (and $[Zn(L^4)]^+$).

The resulting intermediate, containing an O-coordinated ketyl radical anion, is proposed to undergo a rapid intramolecular one-electron transfer with formation of a bound aldehyde, which is a poor ligand and dissociates. The ultimate electron acceptor of this step is the *o*-diiminoquinone unit of the doubly protonated ligand H_2L^3, which is reduced to $[H_2L^2]^-$. Mechanistically, it is conceivable that, in the case of the copper(II)-containing catayst, this ion is the primary electron acceptor, which is thereby reduced to Cu(I) and then intramolecularly reoxidized to Cu^{II} with formation of coordinated $[H_2L^2]^-$. In the case of $[Zn(L^4)]^+$, this is not possible. We have no experimental evidence for either pathway, as these steps follow the rate-determining H-abstraction step.

After the intramolecular oxidation of the ketyl radical anion and dissociation of the aldehyde, the catalysts are in the reduced $[M^{II}(L^2H_2)]^+$ (M^{II} = Cu, Zn) state, where most likely the two phenolates are protonated (or 2 equiv of $[HNEt_3]^+$ has been formed). The reduced catalysts react with dioxygen, yielding H_2O_2 and $[M(L^4)]^+$—the active catalyst. This reoxidation step most probably is also broken down into two successive one-electron-transfer steps, where a coordinated superoxide metal(II) intermediate is formed (eq 18). Such a diamagnetic

$$[M^{II}(L^2H_2)]^+ + O_2 \rightarrow [M^{II}(L^3H_2)(O_2^{\bullet -})]^+ \rightarrow [M^{II}(L^4)]^+ + H_2O_2 \quad (18)$$

intermediate has recently been studied.[7] It has been shown that, in THF solution, the following equilibria (eq 19) exist, where

(13) Halfen, J. A.; Young, V. G., Jr.; Tolman, W. B. *Angew. Chem., Int. Ed. Engl.* **1996**, *35*, 1687.
(14) (a) Stewart, R. *J. Am. Chem. Soc.* **1957**, *79*, 3057. (b) Stewart, R.; van Linden, R. *Discuss. Faraday Soc.* **1960**, *29*, 211.
(15) Lee, D. G.; van den Engh, M. *Can. J. Chem.* **1972**, *50*, 2000.
(16) Roecker, L.; Meyer, T. J. *J. Am. Chem. Soc.* **1987**, *109*, 746.
(17) Thompson, M. S.; Meyer, T. J. *J. Am. Chem. Soc.* **1982**, *104*, 4106.
(18) Lebeau, E. L.; Meyer, T. J. *Inorg. Chem.* **1999**, *38*, 2174.
(19) (a) Cha, Y.; Murray, C. J.; Klinman, J. P. *Science* **1989**, *243*, 1325. (b) Bell, R. P. *The Tunnel Effect in Chemistry*; Chapman and Hall: New York, 1980.
(20) Wachter, R. M.; Branchaud, B. P. *Biochim. Biophys. Acta* **1998**, *1384*, 43.

$H_3(L^c)$ and $H_2(L^b)$ represent the tridentate ligand *N,N′*-bis(2-hydroxy-3,5-di-*tert*-butylphenyl)amine and its monooxidized radical form, respectively.

$$[Cu^{I}(L^{c}H_2)(NEt_3)] + O_2 \rightleftharpoons [Cu^{II}(L^{c}H_2)(O_2^{\bullet -})(NEt_3)] \rightleftharpoons [Cu^{II}(L^{b})(NEt_3)] + H_2O_2 \quad (19)$$

Conclusion

We presented in this work two catalysts, $[M(L^4)]PF_6$ (M = Cu, Zn), which effectively catalyze the aerobic oxidation of primary alcohols, including ethanol and methanol, with formation of the corresponding aldehydes and H_2O_2 at ambient temperature. Up to $\sim 5 \times 10^3$ turnovers in 50 h have been achieved for the air oxidation of ethanol by $[Cu(L^4)]^+$, which corresponds to a turnover frequency of $\sim 0.03\ s^{-1}$. In contrast, the zinc analogue is less efficient, and the catalyst stability is inferior (170 turnovers in 24 h corresponds to a turnover frequency of $0.002\ s^{-1}$). This reactivity difference reflects the fact that the intramolecular rate constant for H-abstraction is faster by a factor of ~10 for the copper-containing catalyst than for its zinc analogue. None of the previously reported catalysts[5b,6,7] is capable of oxidizing methanol. The catalysts $[M(L^4)]^+$ (M = Cu, Zn) are the most effective and stable ones (with respect to decomposition during turnover) reported to date, but overall the process is slow.

Experimental Section

***N,N′*-Bis(3,5-di-*tert*-butyl-2-hydroxyphenyl)-1,2-phenylenediamine (H_4L^1).** A solution of 3,5-di-*tert*-butylcatechol (8.9 g; 4.0 mmol), *o*-phenylenediamine (2.06 g; 2.0 mmol), and triethylamine (0.4 mL) in *n*-heptane (120 mL) was stirred at ambient temperature in an open vessel for 4 d, after which time a pale yellow precipitate was collected by filtration and washed with *n*-pentane. Yield: 4.6 g (44%). ^{1}H NMR (250 MHz, $CDCl_3$): δ 1.30 (s, 18H), 1.48 (s, 18H), 5.30 (b, 2H), 5.85 (b, 2H), multiplet 6.70 (b), 6.92 (b), 7.18 (b) (8H). $^{13}C\{^1H\}$ NMR (62.89 MHz, $CDCl_3$): δ 29.69, 31.62, 34.48, 34.87, 117.46, 118.72, 120.41, 122.20, 128.82, 135.47, 142.65, 147.09. ESI MS: calcd for $C_{34}H_{48}N_2O_2$ 516.8, found 516.3. Anal. Calcd for $C_{34}H_{48}N_2O_2$: C, 79.02; H, 9.36; N, 5.42. Found: C, 78.86; H, 9.40; N, 5.43.

$[Cu^{II}(L^3)]$. An anaerobic solution of the ligand H_4L^1 (0.52 g; 1.0 mmol), $[Cu^{I}(NCCH_3)_4](ClO_4)$ (0.37 g; 1.0 mmol), and NEt_3 (0.5 mL) in dry methanol (50 mL) was heated to reflux under an Ar blanketing atmosphere for 30 min, after which time the yellow solution was cooled to 20 °C and exposed to air. From the green solution, green microcrystals precipitated within 2 h, which were collected by filtration. Recrystallization of this material from CH_3CN produced green single crystals of $[Cu^{II}(L^3)]\cdot CH_3CN$. Yield: 280 mg (49%). ^{1}H NMR (400 MHz, $CDCl_3$): δ 0.83−1.93 (m, 36H), 6.05−7.61 (m, 4H), 20.8 (s, 1H), 24.6 (s, 1H), 39.1 (s, 1H), −6.2 (s, 1H). Anal. Calcd for $C_{34}H_{44}N_2O_2Cu$: C, 70.86; H, 7.70; N, 4.86. Found: C, 70.42; H, 7.75; N, 4.83.

$[Cu^{II}(L^4)]PF_6$. To a solution of $[Cu^{II}(L^3)]$ (144 mg; 0.25 mmol) in dry CH_2Cl_2 (30 mL) was added ferrocenium hexafluorophosphate (83 mg; 0.25 mmol) at −10 °C. After being stirred for 2 h, the violet clear solution was stored at −20 °C for 12 h, after which time a violet precipitate was collected by filtration. Yield: 40 mg (22%). Anal. Calcd for $C_{34}H_{44}N_2O_2CuPF_6$: C, 56.62; H, 6.15; N, 3.88; Cu, 8.81. Found: C, 56.35; H, 6.14; N, 3.91; Cu, 8.74.

$[Cu^{II}(L^5)](ClO_4)_2$. To a solution of $[Cu^{II}(L^3)]$ (288 mg; 0.5 mmol) in dry CH_2Cl_2 (50 mL) at −20 °C was added $[Ni^{III}(tacn)_2](ClO_4)_3$ (615 mg; 1.0 mmol),[9] whereupon the color of the solution changed to deep red within 2 min and to carmine red after 6 h at −20 °C. After filtration, this solution was kept at −80 °C for 10 h, during which time 30 mg of a red-brown microcrystalline material precipitated, which was filtered off at −50 °C and discarded. The resulting solution was stored at −80 °C for 48 h, during which time a red precipitate formed. Yield: 83 mg (21%). Anal. Calcd for $C_{34}H_{44}N_2O_{10}Cl_2Cu$: C, 52.68; H, 5.72; N, 3.61; Cu, 8.20. Found: C, 52.46; H, 5.70; N, 3.60; Cu, 8.29.

$[Zn^{II}(L^3)]$. A solution of $Zn(BF_4)_2\cdot 2H_2O$ (239 mg; 1.0 mmol), the ligand H_4L^1 (516 mg, 1.0 mmol), and NEt_3 (0.5 mL) in dry methanol (50 mL) was heated to reflux under an argon atmosphere for 30 min. After cooling of the yellow solution to 20 °C, it was exposed to air with stirring, whereupon the color changed to deep green. Within 24 h at ambient temperature, microcrystalline gray-black crystals formed, which were collected by filtration. Recrystallization from acetonitrile yielded single crystals of $[Zn(L^4)]\cdot CH_3CN$. Yield: 320 mg (62%). ^{1}H NMR (400 Hz, $CDCl_3$): δ 1.19 (s, 18H), 1.21 (s, 18H), 6.41 (m, 2H), 6.69 (m, 2H), 6.72 (b, 2H), 7.08 (d, J = 1.7 Hz, 2H). The signals at 6.41 and 6.69 ppm form an AA′XX′ system, which was satisfactorily simulated with the following coupling constants: $J_{AA'} = 9.8$ Hz, $J_{A'X'} = 6.8$ Hz, $J_{AX'} = 1.5$ Hz, $J_{AX} = 1.3$ Hz. $^{13}C\{^1H\}$ NMR (100.6 MHz, $CDCl_3$): δ 29.39, 31.30, 34.33, 35.18, 116.36, 122.65, 126.29, 129.61, 136.02, 140.02. Anal. Calcd for $C_{34}H_{44}N_2O_2Zn$: C, 70.64; H, 7.67; N, 4.85; Zn, 11.31. Found: C, 70.45; H, 7.66; N, 4.86; Zn, 11.53.

$[Zn^{II}(L^4)](PF_6)$. A solution of $[Zn(L^3)]$ (146 mg; 0.25 mmol) and ferrocenium hexafluorophosphate (83 mg; 0.25 mmol) in dry CH_2Cl_2 (30 mL) under an Ar atmosphere was stirred at −10 °C for 2 h and then stored at −80 °C for 12 h. A green microcrystalline precipitate formed, which was collected by filtration. Yield: 63 mg (35%). ^{1}H NMR (400 MHz, $CDCl_3$): δ −5.11 (1H), −1.19 (1H), 1.10 (1H), 1.39 (9H), 1.89 (9H), 6.46 (2H), 7.23 (1H), 8.29 (1H), 18.04 (1H), 34.87 (1H), 55.38 (1H), 56.13 (1H). Anal. Calcd for $C_{34}H_{44}N_2O_2PF_6Zn$: C, 56.47; H, 6.13; N, 3.88; Zn, 9.04. Found: C, 56.28; H, 6.15; N, 3.85; Zn, 8.89.

$[Zn^{II}(L^5)](ClO_4)_2$. A solution of $[Zn(L^3)]$ (578 mg; 1.0 mmol) in dry CH_2Cl_2 (100 mL) was photolyzed for 1.5 h at ambient temperature with a Hg immersion lamp. A color change of the deep blue solution to light red was observed during this time. The volume of the reaction mixture was reduced to 50 mL under reduced pressure at −20 °C, and $[TBA]ClO_4$ (0.68 g; 2 mmol) was added. After the solution was stored at −80 °C for 2 d, a red microcrystalline precipitate had formed, which was collected by filtration at −20 °C. Yield: 80 mg (10%). ^{1}H NMR (400 Hz, $CDCl_3$): δ 0.97 (s, 18H), 1.18 (s, 18H), 6.78 (m, 2H), 7.00 (b, 2H), 7.07 (b, 2H), 7.33 (m, 2H). The signals at 6.78 and 7.33 ppm form an AA′XX′ system, which was satisfactorily simulated with the coupling constants: $J_{AA'} = 9.4$ Hz, $J_{A'X'} = 6.2$ Hz, $J_{AX'} = 1.1$ Hz, $J_{AX} = 1.1$ Hz. $^{13}C\{^1H\}$ NMR (62.9 MHz, $CDCl_3$): δ 29.04, 31.08, 34.14, 34.55, 114.97, 123.52, 126.94, 129.90, 131.75, 138.53, 138.86, 144.78, 160.38. Anal. Calcd for $C_{34}H_{44}N_2O_{10}ZnCl_2$: C, 52.55; H, 5.70; N, 3.61. Found: C, 52.36; H, 5.72; N, 3.57.

$[Cu^{II}(H_2L^1)]$. To degassed solution of H_4L^1 (517 mg; 1.0 mmol) and $Cu^{II}(ClO_4)_2\cdot 6H_2O$ (370 mg; 1.0 mmol) in dry, freshly distilled CH_3OH (50 mL) was added NEt_3 (280 μL) under an Ar blanketing atmosphere. After the solution was stirred for 30 min at 20 °C, a brown precipitate had formed in ~70% yield. Anal. Calcd for $C_{34}H_{46}N_2O_2Cu$: C, 70.62; H, 8.02; N, 4.84; Cu, 10.99. Found: C, 70.49; H, 7.95; N, 4.83; Cu, 10.83. The complex is air-sensitive and was stored under an Ar atmosphere.

$[Zn^{II}(H_2L^1)]$. This compound was prepared as described above for $[Cu^{II}(H_2L^1)]$ by using $Zn(ClO_4)_2\cdot 6H_2O$ (1.0 mmol) instead of $Cu(ClO_4)_2\cdot 6H_2O$. Yield: 385 mg (67%). This yellow-brown compound is air sensitive and was stored under an Ar atmosphere. ^{1}H NMR (400 MHz, $CDCl_3$): δ 1.27 (s, 18H), 1.44 (s, 18H), 5.21 (broad s, 2H), 5.9 (very broad, ~1H), 6.69 (s, br, 2H), 6.90 (overlapping s, br, 4H), 7.14 (s, br, 2H). $^{13}C\{^1H\}$ NMR (100.6 MHz, $CDCl_3$): δ 147.0, 142.6, 135.4, 128.8, 122.2, 120.4, 118.7, 117.5, 34.9, 34.4, 31.6, 29.7. Anal. Calcd for $C_{34}H_{46}N_2O_2Zn$: C, 70.39; H, 7.99; N, 4.83; Zn, 11.27. Found: C, 70.11; H, 7.98; N, 4.85; Zn, 10.99.

Kinetic Measurements and Product Analyses. The kinetics of the reactions of complexes $[M(L^4)]^+$ (M = Cu, Zn) with methanol and ethanol under anaerobic conditions in CH_2Cl_2 at 22 ± 1 °C were measured spectrophotometrically using pseudo-first-order conditions (excess alcohol). Pseudo-first-order rate constants were obtained from plots of $\ln(A_t - A_\infty)$ vs time, where A_t is the absorbance at time t and A_∞ is the absorbance of the solution after completion of the reaction. Such plots were linear for 4−5 half-lives.

Table 6. Crystallographic Data

	$[Cu(L^3)]\cdot CH_3CN$	$[Zn(L^3)]\cdot CH_3CN$
chem formula	$C_{36}H_{47}CuN_3O_2$	$C_{36}H_{47}N_3O_2Zn$
fw	617.31	619.14
space group	$P\bar{1}$	$P\bar{1}$
a, Å	10.156(1)	10.173(1)
b, Å	10.435(1)	10.440(1)
c, Å	16.845(2)	16.856(2)
α, deg	83.97(2)	83.95(2)
β, deg	75.47(2)	75.41(2)
γ, deg	69.06(2)	69.11(2)
V, Å	1613.7(3)	1618.4(3)
Z	2	2
T, K	100(2)	100(2)
ρ_{calcd}, g cm^{-3}	1.270	1.271
μ(Mo Kα), cm^{-1}	7.12	7.94
reflns collected	15 017	15 697
unique reflns/[$I > 2\sigma(I)$]	7897/5784	8533/6157
no. of parameters	392	392
$2\theta_{max}$, deg	58.0	60.0
$R1^a$ [$I > 2\sigma(I)$]	0.0455	0.0483
$wR2^b$ [$I > 2\sigma(I)$]	0.1019	0.1111

[a] $R1 = \sum||F_o| - |F_c||/\sum|F_o|$. [b] $wR2 = [\sum[w(F_o^2 - F_c^2)^2]/\sum[w(F_o^2)^2]]^{1/2}$, where $w = 1/\sigma^2(F_o^2) + (aP)^2 + bP$, $P = (F_o^2 + 2F_c^2)/3$.

The kinetics of the catalytic reactions were measured under turnover conditions by spectrophotometric determination of the formation of the products (aldehyde and H_2O_2) using the initial rate method. In all cases, the rates of formation of aldehyde and H_2O_2 were identical within experimental error. The initial rates were obtained by quenching aliquots of the reaction mixture after times t_1, t_2, ..., t_n and analyzing their content of products.

These aliquots were passed through a column containing the ion-exchange resin Amberlyst 15 Dry (Supelco) in order to remove the catalyst. H_2O_2 was determined spectrophotometrically as peroxotitanyl species[21] and, similarly, formaldehyde as 3,5-diacetyl-1,4-dihydrolutidine[10] and acetaldehyde with the reagent 3-methylbenzthiazoline-2-on-hydrazone and $FeCl_3$.[10]

X-ray Crystallographic Data Collection and Refinement of the Structures. Single crystals of $[M(L^3)]\cdot CH_3CN$ (M = Cu, Zn) were selected from the mother liquor with a glass fiber and immediately mounted on a Siemens SMART CCD detector diffractometer, equipped with a cryogenic nitrogen cold stream to prevent loss of solvent. Graphite-monochromated Mo Kα radiation ($\lambda = 0.710\ 73$ Å) was used. Crystallographic data of the compounds are listed in Table 6. Cell constants for **1** and **4** were obtained from a least-squares fit of the setting angles of 5915 and 6182 strong reflections, respectively. Intensity data were collected at −173(2) °C by a hemisphere run taking frames at 0.30° in *ω*. Data were corrected for Lorentz and polarization effects, and a semiempirical absorption correction was carried out using the program SADABS.[22] The Siemens ShelXTL[23] software package was used for solution, refinement, and drawings of the structures. All structures were solved and refined by direct methods and difference Fourier techniques. Neutral atom scattering factors were obtained from literature tables.[24] All non-hydrogen atoms were refined anisotropically. Hydrogen atoms were placed at calculated positions and refined as riding atoms with isotropic displacement parameters.

Physical Measurements. Electronic spectra of complexes and spectra of the spectroelectrochemical investigations were recorded on a Perkin-Elmer Lambda 19 (range 220−1400 nm) and on a HP 8452A diode array spectrophotometer (range 220−820 nm), respectively. Cyclic voltammograms, square-wave voltammograms, and coulometric experiments were performed on EG&G equipment (potentiostat/galvanostat model 273A). Potentials were referenced vs the $Ag/AgNO_3$ electrode, and ferrocene was added as internal standard. EPR spectra of complexes were measured on a Bruker ESP 300E spectrometer equipped with a helium flow cryostat (X-band, Oxford Instruments ESR 910). The solution spectra were simulated with the program written by F. Neese,[25] whereas the spin triplet spectra measured at low temperatures were analyzed on the basis of a spin Hamiltonian description of the electronic ground state:

$$H_e = D[S_z^2 - S(S+1)/3 + (E/D)(S_x^2 - S_y^2)] + \mu_B B\cdot\bar{g}\cdot S \quad (20)$$

where $S = 1$ is the spin of the coupled system and D and E/D are the axial and rhombic zero-field parameters. These simulations were performed with a program which was developed from the $S = {}^5/_2$ routines of Gaffney and Silverstone[26] and which specifically makes use of the calculation of transition fields based on a Newton−Rapshon iterative method as described there. Temperature-dependent magnetic susceptibilities of powdered samples were measured by using a SQUID magnetometer (Quantum Design) at 1.0 T in the range 2−300 K. For calculations of the molar magnetic susceptibility, the raw data were corrected for underlying diamagnetism of the sample by using tabulated Pascal's constants. NMR spectra were recorded on Bruker DRX 400 and DRX 500 instruments.

Acknowledgment. We thank the Fonds der Chemischen Industrie and the Degussa-Hüls (Frankfurt, Germany) for financial support. We thank F. Reikowski for recording the EPR spectra.

Supporting Information Available: Figures S1−S3, showing EPR spectra of $[Cu(L^3)]$, $[Cu(H_2L^1)]$, and $[Cu(L^4)]PF_6$, respectively, Figure S4, showing the temperature dependence of the half-field EPR signal of $[Cu(L^4)]PF_6$ in frozen CH_2Cl_2 solution, and Figure S5, showing the EPR spectrum of $[Cu(L^5)](ClO_4)_2$; tables of crystallographic and structure refinement data, atom coordinates, bond lengths and angles, anisotropic thermal parameters, and calculated positional parameters of H atoms for complexes $[M(L^3)]\cdot CH_3CN$ (M = Cu, Zn) (PDF). An X-ray crystallographic file, in CIF format, is also available. This material is available free of charge via the Internet at http://pubs.acs.org.

JA991481T

(21) Eisenberg, G. M. *Anal. Chem.* **1943**, *15*, 327.
(22) Sheldrick, G. M., Universität Göttingen, 1994.
(23) *ShelXTL* V5.03; Siemens Analytical X-ray Instruments, Inc.: Maddison, WI, 1995.
(24) *International Tables for X-ray Crystallography*; Kynoch Press: Birmingham, U.K., 1991.
(25) Neese, F. Computer program EPR, DOS Version, University of Konstanz, Germany, 1993.
(26) Gaffney, B. J.; Silverstone, H. J. Simulation of the EMR Spectra of High-Spin Iron in Proteins. In *Biological Magnetic Resonance*; Berliner, L. J., Reuben, J., Eds.; Plenum Press: New York, London, 1993; Vol. 13.